THE ASTROPHYSICAL JOURNAL, 372:97–110, 1991 May 1

MULTICOLOR CCD PHOTOMETRY OF GLOBULAR CLUSTERS IN TWO VIRGO ELLIPTICAL GALAXIES

JEAN COUTURE, WILLIAM E. HARRIS,[1] AND J. W. B. ALLWRIGHT[1]
Department of Physics, McMaster University, Hamilton, Ontario, Canada L8S 4M1
Received 1990 May 1; accepted 1990 October 8

ABSTRACT

We present new CCD photometry in the *BVI* system for a sample of globular clusters in NGC 4472, and in *BV* for NGC 4649. Both of these represent "normal" globular cluster systems in giant elliptical galaxies. Just as in the Virgo central giant M87, we find that the clusters in both these galaxies show a large dispersion in color (corresponding to $\sigma([Fe/H]) \simeq 0.6$) at any radius from the center, and that they are distinctly bluer ($\Delta([Fe/H]) \simeq 0.5$) than the integrated halo light. However, quite unlike M87, we find a clear *radial gradient* in the mean cluster colors in both NGC 4472 and 4649, suggesting that the role of dissipational collapse was more important in their formation than it was in M87.

Subject headings: clusters: globular — galaxies: individual (NGC 4472, NGC 4649) — photometry — stars: abundances

1. INTRODUCTION

The study of globular clusters in external galaxies provides an important probe into the events during galaxy formation. In E galaxies particularly, globular clusters probably contain the oldest visible stellar population (Harris 1986, 1988) and are measurable (at least in principle) in samples dozens of times larger than the system of only ~150 clusters within our own Milky Way. In addition, the clusters form a uniform and more narrowly defined stellar population than the uncertain mix making up the halo and central spheroid.

A useful first-order indicator of the heavy-element enrichment processes during formation is the integrated color of the clusters in suitably chosen bandpasses: with modern CCD photometry, color indices are efficiently obtained, and by using globular clusters the color/metallicity gradient of the halo can be traced to much larger radii than is easily done with the halo light. Pioneering work of this type was carried out for selected Virgo ellipticals by Hanes (1971), Ables, Newell, & O'Neil (1974), Strom et al. (1981), and Forte, Strom, & Strom (1981). The latter two studies, with photographic photometry, claimed the detection of abundance gradients in the halos of these galaxies, but later CCD studies (see below) did not confirm this result; it seems likely that the difficulties of photometric calibration in the presence of nonuniform background on photographic plates may have led to small zero-point shifts with position in the color index scales. In the supergiant M87 cluster system, which not surprisingly has been subjected to the most frequent study, multicolor CCD photometry (Cohen 1988; Couture, Harris, & Allwright 1990, hereafter Paper I) strongly suggests that the cluster metallicities are essentially independent of location within the galaxy. However, a legitimate concern is that M87, the prototypical high–specific-frequency system, is by definition unusual, and that we need to extend such work to other more normal galaxies that should tell us more about the *average* processes of formation in large E galaxies.

In this paper, we use new *BVI* photometry to deduce some of the properties of the globular clusters in two large "normal" Virgo elliptical galaxies, NGC 4472 and 4649. The analysis will include the mean cluster color, the dispersion in color or metallicity, and the gradients (if any) with position. Section 2 below presents the observations and data reduction; section 3 the photometric calibration and background estimation; section 4 some comparisons with previous work; and a discussion of the new results in section 5.

2. OBSERVATIONS

The observations reported here were obtained along with our M87 data (Paper I) at the Canada-France-Hawaii Telescope in 1986 March and April. The RCA1 CCD camera was used at prime focus (320 × 512 pixels with a scale of 0.″41 pixel^{-1}). In NGC 4472, a field located ~60″ west of the galaxy center was imaged, and in NGC 4649 a field ~60″ east of center. During the night of 1986 April 2 UT, we obtained a 4 × 700 s series of frames in *V* and a 7 × 350 s series in *I* for NGC 4472, and a 5 × 700 s series in *V* for NGC 4649. (Our intention to add *I*-band images for NGC 4649, and to continue to other galaxies, was unfortunately terminated by weather.) On all of the frames that we did obtain, the seeing was in the range 1.″0–1.″2. The *B* frames for both galaxies are the same ones used for the deep luminosity function study of the globular clusters and for the Virgo nova detection program discussed elsewhere (Pritchet & van den Bergh 1987; Harris et al. 1991), and they cover essentially the same field as our *VI* frames.

The image preprocessing was carried out in the same way as described in Paper I (normal bias subtraction and trim, flat-fielding, and fringe removal in the *I* frames by subtraction of a master "fringe frame" constructed from the median of a series of shifted exposures of background fields). Finally, the halo light of each galaxy was removed by iterated median filter operations (as described in detail in Paper I), and all the frames in each sequence were realigned and averaged. Figure 1 shows the final *V* frames of both our program fields.

We used the DAOPHOT package (Stetson 1987) implemented in its IRAF beta-release version to complete the photometry: (1) The FIND routine was used with a threshold value $\simeq 4\sigma_S$ where σ_S is the mean standard deviation of the sky; the

[1] Visiting Observer, Canada-France-Hawaii Telescope, operated by the National Research Council of Canada, le Centre National de la Recherche Scientifique de France, and the University of Hawaii.

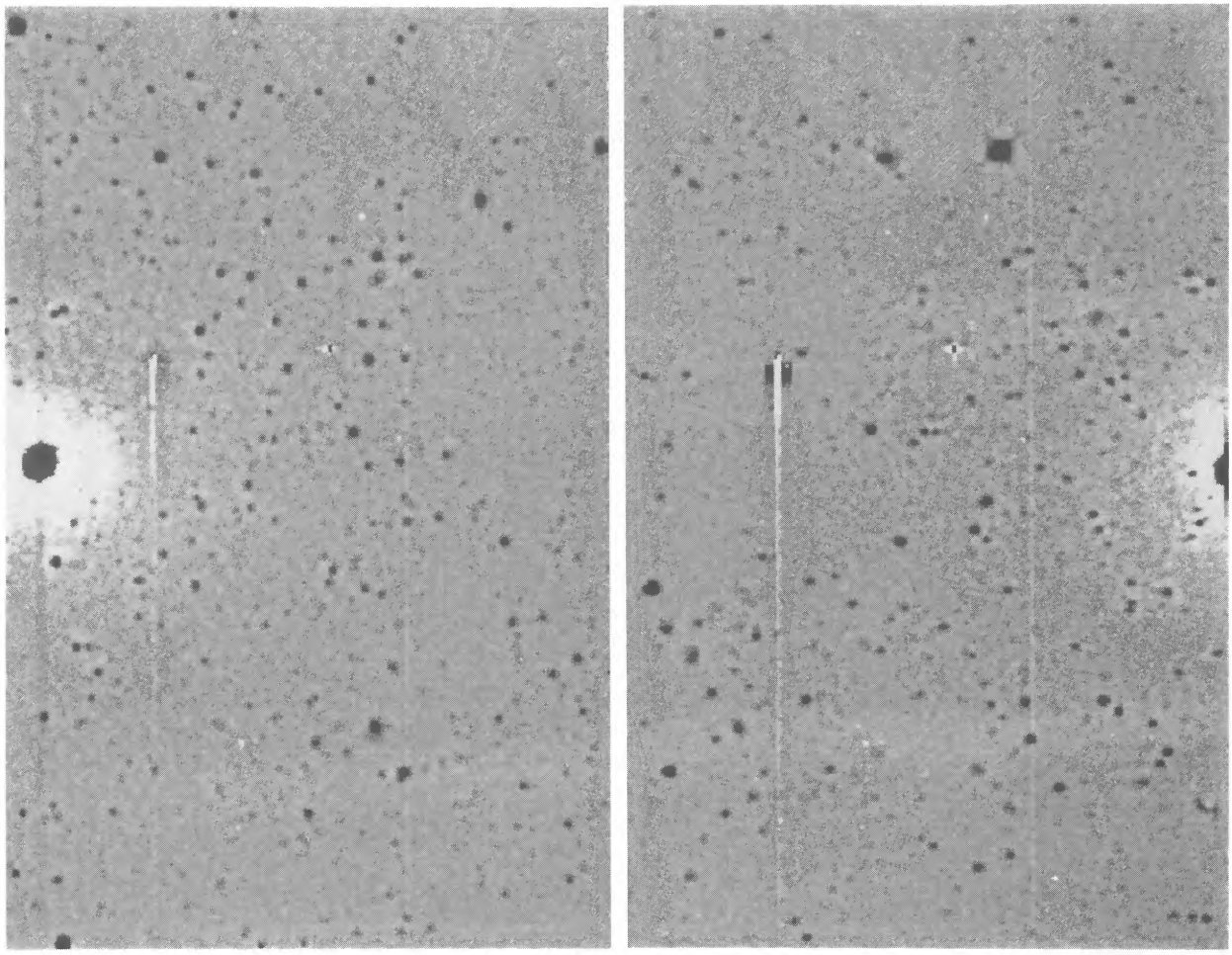

FIG. 1.—CCD composite V frames of the region west of the NGC 4472 nucleus (at the left) and east of the NGC 4649 nucleus (at the right). The background halo light from the galaxies has been removed by median filtering. Each field has dimensions 2.'1 × 3.'4. North is at the top, and east is at the left while ($x = 0$, $y = 0$) is the upper right corner.

very noisy regions of the frames closer than $r \simeq 30''$ from galaxy center were excluded from measurement. (2) Aperture photometry for each measured object was then computed by the PHOT subroutine. Local sky background was determined within an annulus of radii 12 pixels (5″) and 17 pixels (7″). IRAF/APPHOT provides several options for sky level estimation; we tested results from the "mode" and "centroid" (intensity-weighted mean) options on both the median filtered frames and original (with galaxy light present) frames, and eventually chose to use the centroid calculation. The choice is not important for *relative* magnitudes on the frame, since these are determined by PSF profile fitting at small radii (see below), and the measured objects are relatively bright in any case. However, large-aperture photometry is necessary for the scale zero-point calibration (see below), and for this the choice makes some difference since the median filtering operation slightly changes the distribution of sky pixels. (3) A point spread function (PSF) was constructed for each frame from the sum of about five bright isolated starlike images. The deduced sizes of the PSFs were 1.″0 and 1.″1 FWHM, respectively, for the V and I frames of NGC 4472, and 1.″1 FWHM for the V frame of NGC 4649. (4) PSF–fitted magnitudes were derived for all objects on the frames with the usual GROUP and NSTAR subroutines. Three iterations of the FIND/PHOT/NSTAR/SUBSTAR sequence were performed, although the first two passes normally captured ~98% of the total number of real objects. We discarded clearly nonstellar objects from the lists (see Paper I for a description of the image classification procedure) and finally merged the detection lists from each color, keeping only the objects detected in all bandpasses (BVI for NGC 4472, BV for NGC 4649).

3. CALIBRATION, PHOTOMETRIC UNCERTAINTIES, AND BACKGROUND

The calibration of the B data is described fully by Pritchet & van den Bergh (1987) and Harris et al. (1991). For V and I, calibration was made by measurement of standard stars from Landolt (1973, 1983) and Schild (1983) through "large" apertures of radius 10 pixels containing ~97% of the star light. The extinction was measured each night, and mean values over all nights of the run were used for color transformation terms (see Paper I). After removal of extinction and color transformation terms, the zero points from the galaxy program frames were set in the usual way (Stetson 1987) by measuring large-aperture magnitudes m_{ap} for selected bright, isolated starlike objects and finding the mean correction $\langle m_{psf} - m_{ap} \rangle$ for each frame. The mean uncertainties in the photometric zero points, combining the scatter of the mean relations for the standards and the

internal uncertainties in m_{psf} and m_{ap} in the galaxy fields, are $\sigma(B-V) = \pm 0.059$ and $\sigma(V-I) = \pm 0.061$ for NGC 4472 and $\sigma(B-V) = \pm 0.066$ for NGC 4649. These values are significantly larger than those quoted in Paper I for M87 ($\sigma \sim 0.04$), principally because of the scarcity of bright starlike objects suitable for the aperture-correction step in these fields (four or five per frame compared to ~ 12 for M87). Furthermore, any errors can easily differ in size from one field to another. The transfer from the internal NSTAR magnitudes to the large-aperture magnitude scale is therefore, we believe, the dominant source of *external* scale uncertainty in our calibration, and (as will be seen in § 5 below) adversely affects certain comparisons between the globular cluster systems.

The *internal* uncertainties of the photometry were evaluated through DAOPHOT with ADDSTAR experiments in the same manner as described in Paper I. These results are shown in Table 1. The successive columns give the standard deviation σ_V or σ_I of the magnitude residuals (measured minus input) and the number of artificial objects recovered (out of 50 put into the frame) for each color and galaxy. (Note that the B frames, reduced as described in Harris et al. 1991, extend much deeper than the V or I data and contribute negligible photometric error or incompleteness at the levels of interest here. The σ_B values in Table 1 are taken from their paper.) Table 1 shows that some level of incompleteness exists at all magnitudes because of crowding or near-edge locations, with only a small increase toward the faint end of our range.

From the results in Table 1, we estimate that our useful limiting magnitude for color-index purposes should be near $V \simeq 22.5$. This limit is half a magnitude fainter than in Paper I for M87 and is, apparently, due to the better seeing and lower level of crowding in these two galaxy fields. We list our final BVI data for the NGC 4472 field in Table 2 (230 objects) and for the NGC 4649 field in Table 3 (296 objects). These lists contain all the objects with measured BVI (or BV for NGC 4649) colors, although for most purposes in the following discussion only those brighter than the limit mentioned above will be employed. Both tables include the position (x, y) in seconds of arc, the radial distance from the center of the parent galaxy, the V magnitude, and the color indices. The x-coordinates increase from west to east while y increases from north to south. The radial distances for NGC 4649 were computed from an extrapolation of the profile of the galaxy since its center is just out of the frame; the r-values may then have uncertainties of $\sim \pm 2''$.

The lists of Tables 2 and 3 are still contaminated by some foreground stars and small, near-stellar faint background galaxies. As stated in Paper I, the field covered by our frames is too small to estimate accurately the level of this background contamination. However, useful guidance can be obtained from the study of Cohen (1988), who has established a relation giving the number of background objects for a given g magnitude from areas of her frames near NGC 4472 and NGC 4406. For $g < 22.7$ (corresponding approximately to $V < 22.5$), this relation predicts a surface density of 4.6 background objects per arcmin^2. If we normalize to our effective area (rejecting a band 5 pixels wide around the edges of our frames and the region located within 30″ from the center of each galaxy), we estimate ~ 30 background objects in each of our frames brighter than $V \simeq 22.5$. This number should be considered an upper limit to our background level, because of our more stringent rejection criteria.

Harris et al. (1991) have also estimated deep B-magnitude counts in background fields within the Virgo area. Since the data reduction and the removal of extended objects have been done in the same way as we did, their counts should be more relevant than what we deduced from Cohen's relation. Normalizing to the area of our frames and using an equivalent B limiting magnitude, we get about seven background stars per frame. Harris et al. have also computed the B luminosity functions of objects in NGC 4472 and NGC 4649 fields to a much deeper level ($B = 26.2$) than we have obtained here. Since our data cover exactly the same fields, we have compared directly our counts. With the same limiting magnitude, we obtain about the same estimated cluster population for both galaxies if we compare their counts *after subtraction of their background* with our counts *after removal of objects with extreme colors* (see § 5) for the definition of the acceptable color ranges). We conclude that the contribution of background objects in Tables 2 and 3 is at the level of a few percent (at least down to our limiting magnitude) and that most foreground stars in our frames can be excluded on the basis of their color. The discrepancy with the result obtained with Cohen's relation is large but can be explained by the different reduction procedure and, in particular, by the different prescription for the removal of extended objects.

TABLE 1

PHOTOMETRIC UNCERTAINTIES

Magnitude	σ_B (4472–4649)	σ_V (4472)	N_{stars} (4472)	σ_V (4649)	N_{stars} (4649)	σ_I (4472)	N_{stars} (4472)
20.5.....	...	...	...	...	...	0.065	47
21.0.....	...	...	...	...	...	0.081	49
21.5.....	...	0.028	47	0.043	47	0.121	46
22.0.....	0.011	0.056	48	0.083	48	0.181	42
22.5.....	0.014	0.112	46	0.090	48	0.298	47
23.0.....	0.017	0.100	47	0.212	47	...	...
23.5.....	0.023	0.168	45	0.217	44	...	...
24.0.....	0.030	0.208	42	0.270	47	...	...

4. COMPARISONS WITH PREVIOUS DATA

4.1. *Comparison of Counts*

The comparison of our cluster totals with other studies can provide a check on selection effects. As we have just discussed above, the comparison with Harris et al. (1991) is good, although this is not very surprising since both studies used the same fields and the same data reduction (and since our limiting magnitude is bright). We are not aware of any other CCD material for NGC 4649, but for NGC 4472 a good comparison is again possible through the data of Cohen (1988), who performed counts of objects in her entire field up to 4′ from the center of NGC 4472 (our data include only the west portion of her field up to $r \sim 130''$). The results are shown in Table 4 for objects with $V \leq 22.5$ (corresponding to $g \leq 22.7$) for the three zones defined in her paper. For both series of counts, nonstellar objects have been removed as already described, but no subtraction of background population has been made. A glimpse at the table reveals that our densities are lower by $\sim 20\%$ for the two inner regions and by $\sim 30\%$ for the outer one. For M87 (Paper I) we found a discrepancy with Cohen's inner zone but almost perfect agreement for the outer two regions. The present difference in the outermost NGC 4472 zone is not statistically significant (based on only two objects in our overlap region!); the discrepancy in the other regions might be

TABLE 2

BVI PHOTOMETRY OF NGC 4472 GLOBULAR CLUSTERS

#	X	Y	Dist.	V	B-V	V-I
1	80.4	4.0	103.4	21.81	0.71	1.12
2	75.9	4.4	104.9	23.84	1.09	1.51
3	102.3	6.1	94.9	23.53	0.75	0.95
4	125.5	6.4	92.8	17.39	0.72	0.89
5	42.7	7.0	121.0	22.72	0.63	0.83
6	119.0	8.6	90.5	22.39	2.14	1.11
7	45.2	9.3	117.6	21.53	0.53	0.89
8	75.3	10.8	99.5	22.78	0.66	1.29
9	107.9	11.0	89.1	22.66	0.47	0.77
10	119.4	14.5	84.7	23.57	0.87	0.78
11	123.8	15.9	83.2	23.48	0.62	1.50
12	52.9	16.0	107.5	23.84	2.28	3.01
13	89.5	16.7	88.2	22.17	0.64	1.05
14	51.4	17.8	107.1	21.82	0.54	0.96
15	111.6	18.0	81.6	23.14	0.84	1.21
16	13.7	18.9	134.0	22.51	0.74	1.36
17	72.8	19.6	93.0	21.88	0.57	0.98
18	97.6	19.7	82.8	22.18	0.56	0.95
19	62.3	20.4	98.3	22.34	0.76	1.25
20	70.1	21.2	93.2	22.66	0.57	1.00
21	79.2	22.8	87.1	22.51	0.76	1.25
22	86.9	23.3	83.2	21.67	0.55	0.84
23	106.4	23.6	76.9	24.04	0.93	1.30
24	117.8	24.7	74.5	23.46	0.47	1.31
25	110.0	24.9	75.0	23.17	0.82	1.04
26	43.4	25.0	107.4	23.26	0.45	0.96
27	80.5	25.2	84.3	22.39	0.94	1.31
28	113.6	30.4	69.2	22.15	0.74	1.24
29	105.0	30.4	70.5	22.75	0.47	0.99
30	119.0	30.6	68.5	23.48	0.43	1.00
31	18.8	30.6	123.2	23.63	1.51	1.53
32	25.5	30.9	117.5	22.94	0.61	1.28
33	20.8	30.9	121.3	22.90	0.55	0.89
34	122.9	32.8	66.4	23.39	0.62	1.13
35	114.9	33.1	66.3	23.22	0.77	0.98
36	95.6	34.0	69.9	19.83	0.61	1.01
37	121.4	35.3	63.8	23.59	0.82	1.08
38	117.1	35.3	63.9	22.65	0.68	0.98
39	85.0	35.5	73.2	21.87	0.68	1.05
40	128.5	35.8	63.7	22.36	0.85	2.68
41	75.7	37.5	76.5	21.31	0.51	0.87
42	78.3	38.1	74.6	23.89	0.72	1.37
43	65.4	38.4	82.5	23.75	1.70	2.69
44	105.1	39.5	61.7	22.50	0.51	0.94
45	49.3	39.7	93.2	22.59	0.63	0.96
46	73.3	41.0	75.3	23.70	0.75	1.28
47	44.5	41.8	95.7	23.36	0.35	1.00
48	99.8	41.9	61.0	22.86	0.51	1.03
49	28.6	43.5	108.0	19.57	0.11	0.62
50	78.2	43.7	70.1	23.40	0.64	0.92
51	121.2	44.1	55.1	22.62	0.58	0.85
52	45.4	44.8	93.2	22.36	0.55	0.89
53	113.0	45.6	54.1	22.58	0.67	1.04
54	98.7	45.9	57.8	23.00	0.57	0.92
55	73.2	47.8	70.2	22.12	0.68	1.04
56	22.8	49.1	110.3	21.55	0.64	1.24
57	100.3	50.2	53.1	22.98	0.66	1.32
58	113.9	50.9	48.8	23.83	0.60	1.32
59	45.1	51.4	89.8	22.24	0.57	0.96
60	59.4	51.7	77.8	22.50	0.66	1.25
61	92.3	52.2	55.1	22.99	0.64	0.99
62	94.0	52.2	54.1	22.92	0.56	1.16
63	85.2	52.5	58.8	23.85	0.71	1.44
64	103.1	54.5	48.1	23.31	0.78	1.18
65	50.3	55.2	83.3	20.47	0.62	1.06
66	43.3	55.3	89.3	22.82	0.92	1.27
67	99.6	55.8	48.4	23.49	0.79	1.37
68	109.7	56.0	44.6	23.47	0.61	1.08
69	44.9	56.1	87.5	21.81	0.74	1.27
70	97.2	56.2	49.2	22.87	0.62	0.79
71	56.2	56.3	77.8	22.50	0.65	1.20
72	60.6	58.0	73.2	22.86	0.39	1.04
73	82.9	58.6	55.7	21.11	0.76	1.20
74	41.6	59.2	89.0	21.86	0.66	1.08
75	76.9	59.6	59.3	21.42	0.83	1.27
76	66.1	60.9	67.0	21.35	0.54	1.01
77	108.7	63.5	37.7	23.19	0.86	1.08
78	126.1	64.6	34.9	22.65	0.80	0.91
79	78.9	64.9	54.3	22.73	0.65	0.99
80	119.7	65.1	34.0	23.43	1.36	1.13
81	6.4	65.5	119.6	22.64	0.60	1.05
82	116.4	66.6	32.8	22.11	0.51	1.31
83	44.7	66.6	83.1	22.98	0.70	1.24
84	117.9	67.3	32.0	21.71	0.93	1.40
85	84.1	68.0	48.4	22.67	0.79	1.21
86	71.5	68.7	58.2	21.99	0.75	1.38
87	53.4	69.4	74.0	21.75	0.68	1.23
88	49.1	69.8	77.8	22.20	0.76	1.37
89	87.6	70.9	43.9	20.93	0.63	0.95
90	13.0	71.8	111.6	23.33	0.60	1.00
91	85.8	76.1	42.2	22.47	0.68	1.54
92	44.5	77.0	79.8	22.39	0.51	1.19
93	52.1	77.2	72.4	20.63	0.49	1.09
94	9.5	77.6	113.7	23.14	0.83	1.18
95	75.0	78.6	50.4	23.56	0.82	1.08
96	78.7	78.6	47.2	22.98	0.92	1.05
97	69.2	79.0	55.7	21.58	0.54	1.10
98	95.1	79.1	32.8	23.17	2.46	0.78
99	87.4	79.8	38.9	22.79	1.07	1.42
100	91.7	80.9	34.6	23.93	0.35	1.49
101	57.0	84.8	65.7	23.62	0.55	1.14
102	44.5	86.2	77.7	23.06	0.80	1.35
103	58.5	87.0	63.8	22.49	0.64	1.44
104	73.0	88.4	49.3	22.97	0.68	1.33
105	81.1	88.4	41.4	24.22	0.68	1.71
106	84.9	88.6	37.7	23.30	0.77	1.19
107	62.3	91.3	59.4	23.87	0.74	1.70
108	66.1	91.6	55.5	23.37	0.66	1.18
109	89.0	92.0	32.9	22.62	0.60	1.08
110	55.4	92.6	66.0	20.75	0.71	1.20
111	74.4	93.6	47.1	22.93	0.78	1.01
112	71.9	93.7	49.5	22.51	0.79	1.25
113	65.5	94.4	55.8	23.52	0.82	0.91
114	59.9	94.7	61.4	23.66	0.42	0.54
115	77.4	95.5	43.9	23.39	0.76	1.36
116	41.5	95.9	79.7	23.46	0.80	1.11
117	36.0	97.3	85.2	22.06	0.73	1.17
118	82.9	98.0	38.2	23.55	0.66	1.37
119	45.5	98.7	75.6	21.17	0.85	1.30
120	76.7	99.4	44.4	23.52	0.79	1.50
121	52.3	99.8	68.8	22.33	0.61	0.61
122	32.3	103.4	88.9	23.86	0.39	1.39
123	77.5	103.7	43.9	21.47	0.93	1.07
124	44.8	106.3	76.7	22.63	0.34	0.87
125	88.4	106.4	33.6	22.58	0.93	1.07
126	28.4	107.5	93.2	23.09	0.61	1.09
127	77.0	108.6	45.2	22.54	0.36	0.76
128	80.0	109.0	42.3	23.49	1.02	1.32
129	91.6	109.0	31.1	24.50	1.04	1.62
130	30.0	109.1	91.7	23.36	0.75	0.72
131	37.5	110.7	84.4	21.94	0.47	0.93
132	30.0	111.1	91.9	23.88	0.45	1.48
133	72.0	111.2	50.6	22.61	0.86	1.24
134	79.4	111.2	43.5	23.29	0.70	0.85
135	11.7	111.3	110.1	23.01	0.48	1.09
136	44.0	111.5	78.1	21.80	0.45	0.83
137	51.3	112.0	71.0	23.14	0.80	1.32
138	48.1	112.4	74.3	23.65	0.84	1.13
139	56.2	113.0	66.4	23.20	0.73	1.09
140	89.4	115.5	35.8	22.93	0.84	1.25
141	23.9	115.9	98.7	21.02	0.64	1.09
142	12.6	117.9	110.2	23.26	0.81	0.99
143	95.2	118.3	32.3	21.78	0.52	0.82
144	85.2	118.6	40.9	23.10	0.92	1.48
145	61.6	118.9	62.8	23.11	0.81	1.01
146	8.4	119.3	114.5	22.81	0.75	1.02
147	100.0	120.2	29.9	23.67	0.76	1.23
148	98.2	121.5	32.1	23.90	0.22	1.46
149	59.6	121.6	65.5	21.75	0.75	0.98
150	100.6	123.9	32.2	21.73	0.88	1.22
151	104.2	124.1	30.2	24.15	0.37	1.80
152	60.7	124.4	65.5	22.82	0.47	0.21

TABLE 2—*Continued*

#	X	Y	Dist.	V	B-V	V-I	#	X	Y	Dist.	V	B-V	V-I
153	88.6	125.0	41.6	21.52	0.58	0.91	192	34.7	153.1	101.9	23.40	0.75	1.13
154	53.0	125.7	73.1	22.12	0.63	0.81	193	72.1	153.2	73.0	22.81	0.46	0.92
155	97.7	125.9	35.6	25.22	0.57	1.56	194	25.2	153.4	110.2	22.36	0.44	0.92
156	49.5	126.9	76.9	22.64	0.37	0.95	195	84.8	154.1	65.9	23.62	0.83	1.41
157	25.3	127.2	99.9	24.07	0.52	1.63	196	47.9	155.2	92.2	23.97	0.83	1.20
158	99.4	127.5	35.8	23.66	0.86	1.14	197	63.5	158.6	82.8	21.53	0.62	1.01
159	114.2	129.9	31.6	23.26	0.53	0.86	198	57.0	160.5	88.7	22.95	0.69	1.11
160	69.4	130.7	60.6	23.65	0.90	1.30	199	61.0	161.1	86.3	23.91	0.56	1.57
161	100.6	131.6	38.5	22.48	0.75	1.19	200	6.2	162.2	131.1	23.40	0.53	1.35
162	15.6	131.9	110.5	22.39	0.58	0.84	201	102.5	162.4	66.0	23.28	0.96	1.00
163	5.6	132.4	120.3	23.75	0.58	1.39	202	45.1	165.0	100.6	20.28	0.31	0.57
164	22.3	133.1	104.5	21.71	0.81	1.25	203	49.7	165.5	97.5	22.89	0.63	0.60
165	73.9	133.4	58.3	22.73	0.66	0.94	204	20.1	168.0	122.2	22.35	0.67	1.29
166	46.2	133.4	82.4	23.72	0.18	1.63	205	84.0	168.2	78.5	23.51	0.60	0.79
167	95.9	133.4	42.6	23.02	0.87	0.95	206	30.2	169.3	114.8	24.02	0.54	1.65
168	21.1	135.9	106.6	23.87	0.22	1.49	207	106.1	173.1	75.5	22.57	0.72	1.27
169	98.6	136.4	43.5	23.98	0.93	1.13	208	125.0	173.2	74.2	22.06	0.76	1.16
170	111.1	137.9	40.0	22.38	0.61	1.26	209	65.1	173.8	93.4	21.49	0.64	1.16
171	113.6	137.9	39.5	21.67	0.58	0.91	210	76.9	174.0	87.0	23.24	0.43	0.98
172	124.5	139.9	40.9	24.17	0.83	1.36	211	10.7	176.0	134.5	22.06	0.54	0.85
173	56.1	140.1	76.9	23.71	0.77	1.12	212	21.4	176.4	126.2	23.48	0.66	1.33
174	21.0	140.3	108.3	23.81	0.56	1.28	213	53.8	177.9	103.6	23.39	0.80	0.94
175	106.5	140.5	43.9	23.95	0.76	1.15	214	70.3	179.9	95.4	23.63	0.78	1.36
176	8.5	140.7	120.1	21.11	0.67	1.17	215	47.2	179.9	109.5	23.52	0.87	0.93
177	86.6	141.0	54.3	22.46	0.57	0.77	216	7.8	185.5	142.5	23.88	0.80	1.31
178	47.1	142.6	85.8	21.82	0.63	0.84	217	117.9	187.5	88.5	22.26	0.42	1.12
179	109.1	143.3	45.8	21.84	0.81	1.13	218	10.4	187.9	141.9	22.50	0.54	0.80
180	67.5	143.5	69.6	23.75	0.60	1.57	219	83.8	188.4	96.8	23.39	0.64	1.29
181	13.8	144.0	116.4	22.27	0.04	1.34	220	24.0	190.7	133.5	22.85	0.52	0.94
182	110.9	144.9	46.9	23.63	0.25	1.39	221	48.4	191.1	117.2	23.42	0.68	1.25
183	105.0	145.3	48.9	23.40	0.87	0.65	222	122.7	192.9	93.8	23.65	0.63	1.24
184	110.5	148.8	50.8	22.73	0.82	0.97	223	108.7	193.2	94.9	23.49	0.37	1.45
185	63.5	149.0	76.3	22.90	0.87	0.95	224	90.8	193.4	99.0	23.86	1.08	2.87
186	8.6	149.4	123.3	23.68	0.80	0.85	225	44.6	195.8	123.3	23.10	0.80	1.12
187	21.5	149.5	111.7	23.66	0.71	0.80	226	45.9	198.7	124.8	23.00	0.73	0.98
188	64.8	149.9	75.9	22.49	0.77	0.93	227	78.8	199.3	108.8	22.82	0.45	1.04
189	77.5	150.5	67.4	23.10	0.58	1.23	228	66.2	201.2	115.9	22.53	0.38	0.87
190	7.5	151.9	125.3	22.70	0.66	1.10	229	75.1	201.7	112.4	22.66	0.61	1.10
191	120.4	152.8	53.7	21.17	0.69	1.22	230	116.9	201.9	102.9	19.19	0.13	1.04

understood by slightly different net completeness levels, since we include only the images detected in all three colors. An additional effect may be related to the ellipsoidal space distribution of the cluster population as mentioned by Cohen (1988). Since our frames are centered on the minor axis (the major axis of NGC 4472 is almost in the north-south direction), the global effect is to weight our mean number density toward the minor axis and thus to lower values (see Table 9 of Cohen 1988). In the case of M87, its almost spherical shape prevents such an effect.

We have also compared our NGC 4472 counts with the photographic studies of Harris & van den Bergh (1981) and Hanes (1977). The comparisons are necessarily only rough ones in this case, because both studies refer to unique and different magnitude limits and area deliminations. The counts of the former study are higher than those of Cohen by about ~15%–30% (depending on the radial zone), perhaps because the nonstellar objects were not as completely removed in the photographic starcounts. From Hanes's study, we deduced a density of ~4.0 objects per arcmin^{-2} at 2′ from the center of the galaxy, in good agreement with Cohen's value.

4.2. *Comparison of Photometry*

Our *BVI* photometry of NGC 4472 can be directly compared with the *gri* photometry of Cohen (1988), since our field falls entirely within her measured region. Cohen publishes complete data for objects brighter than $g = 22.1$. From this list, we find 40 objects in common with our measurements in Table 2. Using these, we first derive coordinate transformations: if (x_C, y_C) denote the star positions in Cohen's systems, we find the following relations to our values (x, y):

For the region south of the galaxy center ($y_C < 0$):

$$x = (120.2 \pm 0.05) - x_C\ , \quad y = (97.0 \pm 0.05) - y_C\ .$$

For the region north of the galaxy center ($y_C > 0$):

$$x = (124.4 \pm 0.06) - x_C\ , \quad y = (105.7 \pm 0.07) - y_C\ .$$

In all cases the coordinate values are in seconds of arc. Within each of the two segments (north and south) we found the transformations to be very precisely defined, with no need for any scale change or rotation (only simple zero-point shifts in x and y). The ~10″ shift between the northern and southern halves appears to be due to the boundary between two of the adjacent CCD chips in the 4-shooter camera used by Cohen, since in her study the galaxy nucleus was placed nearly on one of the chip edges (see Cohen's discussion, and a similar coordinate comparison made in Harris et al. 1991).

The 40 bright objects found in common were used to derive approximate magnitude and color transformations from $(g, g - r)$ into $(V, B-V)$. The nominal relations according to an earlier paper of Cohen (1985) are

$$V = g - 0.371(g - r) - 0.038\ ,$$

$$(B-V) = 0.963(g - r) + 0.454\ .$$

The actual correlations we find, along with these two equations, are plotted in Figure 2. Although the *slopes* (color terms) appear to represent the relations correctly, the *zero points* in

TABLE 3

BV PHOTOMETRY OF NGC 4649 GLOBULAR CLUSTERS

#	X	Y	Dist.	V	B-V	#	X	Y	Dist.	V	B-V	#	X	Y	Dist.	V	B-V
1	34.6	5.1	101.1	21.75	0.53	51	108.5	50.2	118.8	22.61	0.67	102	70.4	80.2	72.5	23.86	0.81
2	20.8	6.1	96.4	23.38	1.06	52	103.3	51.7	113.5	22.78	0.91	103	33.7	80.3	38.6	21.07	1.09
3	13.7	7.3	94.0	22.98	0.81	53	92.1	54.0	102.4	22.40	0.75	104	125.0	80.4	125.8	21.89	0.65
4	108.9	7.6	142.4	21.40	0.74	54	44.3	54.0	63.6	21.97	0.83	105	24.1	80.9	30.4	21.70	1.43
5	99.0	8.6	134.4	22.18	0.72	55	46.5	54.1	65.1	23.09	0.67	106	123.1	81.0	123.8	23.42	0.54
6	39.7	9.3	99.1	23.30	1.13	56	82.6	54.7	93.7	23.35	0.46	107	73.3	81.5	74.9	23.85	0.30
7	56.2	9.3	106.7	22.43	0.49	57	48.9	56.4	65.2	21.32	0.54	108	62.7	83.0	64.3	24.30	0.49
8	27.3	14.4	90.0	21.98	0.72	58	64.4	56.9	77.1	23.41	0.89	109	30.1	83.4	33.9	22.44	2.36
9	43.0	16.3	94.2	23.95	0.46	59	35.5	57.0	55.5	22.89	0.80	110	70.0	83.5	71.2	23.83	0.62
10	25.5	17.6	86.4	22.83	0.64	60	33.7	58.2	53.5	22.70	1.40	111	46.4	84.4	48.3	22.02	0.99
11	17.6	19.5	82.6	22.84	0.80	61	25.1	58.7	48.3	21.96	0.94	112	75.3	84.4	76.2	23.00	0.66
12	11.9	19.8	81.4	22.94	0.88	62	10.7	58.8	42.8	21.36	0.91	113	48.4	84.9	50.1	22.30	0.52
13	31.2	20.4	85.6	23.81	0.65	63	8.5	58.9	42.3	24.33	0.40	114	56.7	85.2	58.0	22.25	0.60
14	78.6	20.8	111.3	22.61	0.79	64	102.7	60.2	109.5	23.24	0.51	115	67.8	89.1	67.9	24.13	0.62
15	22.9	22.1	81.4	21.18	0.86	65	104.6	60.5	111.2	22.73	0.62	116	62.5	89.4	62.7	23.41	0.96
16	37.5	22.1	86.5	23.65	0.86	66	5.9	60.9	39.9	21.34	0.70	117	81.6	89.5	81.5	23.32	0.23
17	45.0	22.3	89.7	23.48	0.63	67	46.2	61.0	60.2	23.75	0.63	118	31.5	90.3	32.3	22.79	0.64
18	8.4	22.5	78.3	22.91	0.75	68	32.6	61.2	50.5	21.26	0.76	119	49.3	91.3	49.4	23.21	0.64
19	83.7	22.5	113.7	23.44	1.08	69	119.7	61.3	125.2	24.15	1.18	120	77.4	91.7	77.1	21.17	0.20
20	67.7	24.6	101.1	23.68	0.96	70	18.9	61.7	42.7	24.27	0.70	121	66.3	92.3	66.0	22.00	0.80
21	33.9	24.7	82.6	22.24	0.73	71	66.4	62.1	76.0	22.90	0.27	122	63.9	92.3	63.6	22.38	1.00
22	19.9	25.6	77.3	23.71	1.05	72	9.5	62.6	38.8	22.34	0.72	123	108.9	93.3	108.3	23.45	0.49
23	105.3	25.7	128.5	22.65	0.81	73	78.1	63.0	85.9	23.82	0.42	124	85.9	93.5	85.4	23.64	0.54
24	91.4	26.0	117.3	21.78	0.77	74	66.8	64.9	75.0	22.86	0.90	125	68.4	94.5	67.9	21.70	0.69
25	100.6	26.3	124.3	24.05	0.80	75	46.1	66.6	56.5	22.51	0.65	126	74.9	94.7	74.3	24.03	1.11
26	32.3	27.8	79.2	22.91	0.97	76	16.7	67.7	36.4	23.04	1.05	127	57.2	94.8	56.7	23.31	0.92
27	102.0	29.0	123.9	23.18	0.90	77	36.9	68.6	48.1	22.61	2.33	128	120.3	95.0	119.6	22.09	0.65
28	46.6	29.5	84.4	21.53	2.57	78	26.5	68.7	40.8	24.44	1.20	129	85.2	95.9	84.5	23.23	0.92
29	99.9	31.2	120.9	23.29	0.54	79	50.0	68.7	58.6	23.44	0.60	130	45.1	97.4	44.4	24.77	1.46
30	74.6	31.3	101.1	24.25	-0.22	80	41.1	69.6	50.7	22.74	1.60	131	53.0	98.7	52.2	22.48	0.66
31	84.9	31.8	108.6	22.34	0.27	81	39.2	69.7	49.1	21.62	1.03	132	69.1	98.9	68.3	22.97	0.95
32	104.9	33.1	123.9	23.10	0.79	82	68.6	70.0	74.3	23.19	1.83	133	83.6	99.6	82.8	24.12	1.09
33	88.0	35.1	109.0	23.03	0.86	83	24.2	71.4	37.3	21.42	0.66	134	49.9	99.7	49.1	23.59	0.90
34	120.1	35.5	135.8	24.04	0.82	84	57.0	71.4	63.2	23.50	0.98	135	45.7	99.8	44.8	23.40	1.11
35	85.4	36.3	106.2	23.10	0.35	85	37.6	71.9	46.5	22.57	2.03	136	42.0	100.0	41.2	22.23	0.87
36	10.9	36.5	64.8	24.11	0.59	86	14.2	73.0	30.5	24.11	1.65	137	38.9	101.2	38.1	24.20	0.90
37	118.0	36.9	133.3	22.13	0.31	87	61.1	73.1	66.2	22.77	1.40	138	36.3	102.2	35.6	22.18	1.09
38	99.1	37.6	116.6	23.13	0.65	88	57.6	73.6	62.8	22.93	1.32	139	75.2	103.0	74.4	23.32	0.91
39	71.4	38.1	94.2	22.59	1.38	89	43.0	73.8	49.9	24.17	0.74	140	112.1	105.9	111.5	23.62	0.78
40	105.8	38.2	122.0	22.77	0.42	90	48.7	74.3	54.5	22.84	0.71	141	121.8	106.1	121.1	22.44	0.74
41	44.7	39.5	75.1	23.98	0.59	91	36.8	74.5	44.4	21.50	1.04	142	67.4	107.1	66.9	24.38	0.15
42	28.0	40.4	65.9	23.91	0.80	92	26.2	75.1	35.9	23.31	0.52	143	69.3	107.2	68.8	23.34	1.09
43	21.4	42.2	61.8	23.63	0.85	93	92.1	75.6	94.6	21.56	0.88	144	53.3	107.2	52.9	20.28	0.23
44	61.8	43.0	83.8	23.30	0.75	94	51.3	76.3	55.9	22.71	1.09	145	45.5	109.6	45.6	22.94	1.00
45	109.6	44.1	122.5	24.00	0.20	95	73.8	76.4	76.9	23.30	0.85	146	49.3	109.9	49.4	23.69	0.69
46	35.0	45.4	64.8	22.11	0.89	96	31.3	76.8	38.6	22.46	2.00	147	30.8	110.0	31.5	21.67	0.97
47	60.8	46.4	80.7	23.00	1.56	97	24.8	77.8	33.0	22.38	1.59	148	66.5	110.3	66.4	23.31	1.17
48	18.4	47.5	55.8	23.61	0.85	98	43.9	77.9	48.6	23.08	0.67	149	34.5	112.4	35.7	23.91	0.44
49	32.9	47.5	61.9	24.53	0.40	99	127.6	79.4	128.5	23.01	0.74	150	55.7	113.1	56.3	20.88	0.77
50	96.2	49.1	108.3	22.37	0.71	100	56.1	79.6	59.1	23.23	0.63	151	29.7	113.2	31.6	21.95	0.98
						101	116.3	80.1	117.3	22.45	0.58	152	51.8	113.3	52.6	23.74	0.40

each case are ~0.2 mag different from Cohen's values. Adopting the standard color terms and rederiving the constants in the relations, we find

$$V = g - 0.371(g - r) + (0.204 \pm 0.018),$$

$$(B-V) = 0.963(g - r) + (0.250 \pm 0.023),$$

as the actual transformations between the two sets of measurements.

The differences are in the sense that we measure the clusters to be slightly *bluer* and *fainter* than in Cohen's study. Such zero-point shifts could be the main source of the discrepancy noted in Paper I, in which a difference of the same order was suspected for M87 (although in that case we were not able to compare our data directly with Cohen's). A difference in the bandpasses and/or imprecision in the transformation equations (due for example to a difference in metallicity between the standards used to establish the relation and the globular clusters) could contribute to the shift, though we would not expect this to be the whole explanation. Disagreements at the 0.1–0.2 mag level are of no serious importance for luminosity function studies of the clusters (e.g., Grillmair, Pritchet, & van den Bergh 1986; Cohen 1988; Harris et al. 1991), but they are much more of concern in the *color indices* since the mean metallicity differences between clusters in different galaxies show up as color changes at just this level. We are unable at present to assess which (if either) of the two studies represents the more nearly correct scale, and further work designed particularly for external zero point calibration will be required to settle the issue. However, we stress that the *internal* precision of the photometry is quite a different matter and that *relative* differences in color between objects in any one field (see below) can readily be detected.

5. INTEGRATED PROPERTIES OF THE CLUSTER POPULATIONS

5.1. *Color Distributions*

The color distributions of the measured starlike objects are shown in Figures 3–6. As noted previously, these samples include only the objects brighter than $V = 22.5$, avoiding the

TABLE 3—*Continued*

#	X	Y	Dist.	V	B-V	#	X	Y	Dist.	V	B-V	#	X	Y	Dist.	V	B-V
153	103.9	113.5	103.9	23.44	0.61	201	89.8	137.7	96.5	23.16	1.37	249	100.4	164.9	118.6	23.07	0.83
154	53.4	115.3	54.6	21.95	0.81	202	122.4	137.9	127.2	23.42	0.58	250	81.3	165.5	103.4	23.55	0.45
155	71.4	115.6	72.2	20.80	0.67	203	34.9	138.0	50.7	22.20	0.92	251	124.1	166.5	139.9	23.69	0.35
156	27.8	116.3	31.3	22.72	1.57	204	78.5	138.2	86.3	23.59	0.01	252	15.7	166.6	67.8	24.50	1.63
157	24.8	118.2	29.8	23.82	0.81	205	75.7	138.8	84.1	22.22	0.82	253	20.2	167.2	69.5	22.26	0.68
158	56.4	118.3	58.4	23.28	0.90	206	13.6	138.9	40.5	23.91	1.67	254	51.5	167.7	84.2	23.04	0.45
159	98.1	118.8	99.0	23.24	1.07	207	106.6	139.1	112.6	23.50	0.50	255	85.8	168.1	108.6	23.74	0.86
160	100.3	118.9	101.2	22.21	0.57	208	56.6	139.8	68.3	22.71	0.58	256	38.3	168.2	77.4	20.98	0.71
161	86.0	119.4	87.2	24.42	0.40	209	86.9	139.9	94.7	23.52	0.69	257	89.7	169.2	112.4	23.58	0.79
162	38.2	119.6	42.0	22.98	1.32	210	65.6	140.3	76.1	22.92	0.83	258	102.9	169.9	123.5	22.03	1.06
163	29.0	120.7	34.7	23.14	0.90	211	39.2	141.1	55.9	23.49	0.91	259	92.1	170.2	114.9	23.75	0.50
164	62.1	121.1	64.7	23.91	0.28	212	106.4	143.0	113.9	22.75	0.56	260	77.0	170.3	103.4	23.15	0.54
165	85.2	122.9	87.4	22.39	0.79	213	45.3	143.0	61.6	23.09	0.78	261	67.4	170.3	96.5	23.05	0.50
166	90.4	123.9	92.6	21.90	0.55	214	13.0	143.5	44.7	22.30	0.90	262	28.7	172.1	76.9	23.92	0.54
167	23.1	124.5	32.8	22.07	0.78	215	85.0	144.4	95.0	23.73	1.19	263	8.6	172.3	72.2	22.28	0.64
168	19.7	125.1	31.1	23.77	0.94	216	28.6	144.5	52.1	23.24	0.70	264	49.4	172.3	86.7	22.79	0.54
169	123.6	125.4	125.3	18.35	1.32	217	45.4	145.5	63.4	23.45	0.71	265	48.1	172.9	86.5	22.73	0.80
170	104.7	125.9	107.0	23.30	0.73	218	53.9	145.9	69.9	22.67	0.69	266	5.7	173.0	72.7	22.26	0.70
171	48.9	125.9	54.4	21.95	0.79	219	103.2	146.5	112.3	22.40	0.80	267	108.4	173.5	130.0	21.82	0.62
172	15.5	126.6	30.0	21.04	1.62	220	111.3	147.7	120.1	21.55	0.60	268	31.6	173.9	79.7	22.95	0.61
173	126.0	126.6	127.9	22.52	2.68	221	88.2	148.0	99.5	23.67	0.63	269	73.8	174.3	103.8	23.28	1.40
174	100.8	127.5	103.5	24.50	1.10	222	67.5	148.2	82.0	22.44	0.63	270	5.9	174.9	74.6	24.01	1.06
175	24.8	127.7	36.3	24.02	1.00	223	59.1	149.1	76.0	23.67	0.62	271	100.6	177.4	126.0	22.95	0.88
176	121.6	127.8	123.8	21.89	3.69	224	91.3	149.2	102.8	21.42	0.71	272	113.0	178.8	136.9	23.52	0.16
177	29.5	128.3	40.0	23.90	1.11	225	28.8	149.5	56.5	20.55	0.66	273	67.5	178.9	102.9	22.91	0.73
178	22.9	128.6	35.8	21.68	0.72	226	45.3	149.7	66.4	20.99	0.86	274	64.8	180.5	102.4	22.22	1.25
179	81.7	128.8	85.7	22.06	0.55	227	99.9	149.7	110.6	23.42	0.65	275	25.8	181.7	85.0	23.30	0.62
180	16.5	129.1	32.7	23.43	1.13	228	52.5	150.2	71.8	22.43	0.35	276	48.6	182.6	95.0	22.10	0.97
181	109.9	129.8	112.9	23.46	0.62	229	15.6	150.6	52.3	23.70	0.83	277	96.1	182.9	126.0	23.93	0.33
182	70.7	129.8	75.8	22.77	0.54	230	101.5	150.7	112.5	23.47	0.33	278	55.4	184.9	100.6	21.22	0.66
183	23.4	130.3	37.4	21.54	0.75	231	25.7	152.1	57.3	22.31	0.17	279	115.8	186.7	143.8	21.79	0.66
184	59.4	130.3	65.8	23.59	0.57	232	50.0	153.2	72.1	22.69	0.62	280	61.3	187.0	105.6	24.37	0.96
185	11.8	130.4	31.9	22.91	1.23	233	12.2	153.8	54.5	23.25	0.72	281	59.8	189.4	106.7	23.74	0.85
186	111.3	131.6	114.8	23.60	1.13	234	32.7	153.9	62.2	23.47	1.05	282	25.2	189.5	92.3	23.48	0.75
187	73.6	132.1	79.4	22.90	0.40	235	125.5	154.2	135.8	23.09	0.84	283	86.2	189.5	123.4	23.63	0.10
188	88.3	132.8	93.3	24.09	1.00	236	18.5	154.5	56.8	21.77	0.58	284	33.3	193.2	98.2	23.35	1.32
189	113.9	132.9	117.6	22.05	0.77	237	8.1	155.0	55.1	23.66	0.56	285	8.5	194.1	94.0	24.80	1.06
190	105.1	133.8	109.4	22.94	1.24	238	111.8	155.4	123.9	24.05	1.25	286	61.8	194.6	112.2	23.67	0.62
191	62.4	133.8	70.1	21.30	1.27	239	52.1	156.3	75.8	23.04	0.98	287	14.4	195.4	95.9	22.23	0.70
192	120.7	134.0	124.5	20.70	0.81	240	11.0	157.5	57.9	23.92	0.07	288	10.5	195.7	95.7	21.90	0.85
193	101.7	134.1	106.3	23.69	0.73	241	110.4	157.6	123.6	22.21	0.62	289	7.4	195.9	95.7	21.73	0.67
194	43.0	134.1	54.0	23.20	0.78	242	44.3	157.9	72.0	21.03	0.79	290	94.1	196.3	133.8	22.34	0.52
195	97.7	135.3	103.0	22.84	0.44	243	18.8	159.2	61.4	23.69	1.49	291	22.2	197.7	99.6	23.41	0.70
196	101.7	135.8	106.9	21.54	0.79	244	47.4	160.4	75.9	23.73	0.60	292	71.3	199.0	121.2	23.99	0.55
197	68.9	136.1	76.8	23.39	0.92	245	15.5	160.4	61.7	20.97	0.68	293	44.1	199.0	107.6	23.10	0.36
198	73.9	136.3	81.4	23.65	0.84	246	17.1	163.1	64.7	21.85	0.60	294	91.4	199.9	134.5	21.91	0.58
199	79.5	137.1	86.8	23.31	0.92	247	86.5	164.1	106.7	21.78	0.71	295	33.6	200.4	105.2	23.33	0.37
200	10.4	137.3	38.1	24.70	2.12	248	120.2	164.4	135.4	19.67	0.71	296	42.4	200.7	108.6	24.44	0.70

fainter images with less precise photometry; and at most about one-third of the objects making up the histograms are from field contamination (most noticeable at extreme colors away from the center of the distribution). The main parameters of the color distributions are given in Table 5, where σ represents the global dispersion of the distributions, σ_{obs} the dispersion expected from the uncertainties of the photometry (Table 1), and σ_0 the "true" residual dispersion of the population (i.e., $\sigma_0^2 = \sigma^2 - \sigma_{obs}^2$). Figures 3–6 have been used along with the calibration diagram of intrinsic colors in Paper I to narrow the color limits defining the globular cluster populations to remove objects with extreme colors. Therefore only objects located in the following ranges:

$$\text{for NGC 4472:}\quad 0.3 \le (B-V) \le 1.1\ ,$$
$$0.7 \le (V-I) \le 1.6\ ,$$
$$1.3 \le (B-I) \le 2.2\ ;$$
$$\text{for NGC 4649:}\quad 0.4 \le (B-V) \le 1.2\ ,$$

have been included in the statistical computations of Table 5. These color limits generously include all known globular clus-

TABLE 4

COMPARISON OF COUNT DENSITIES FOR NGC 4472

Area	$\text{Density}_{\text{Cohen}}$ (objects per arcmin^2)	$\text{Density}_{\text{CHA}}$ (objects per arcmin^2)
$25'' < r \le 60''$	17.9	14.1
$60'' < r \le 130''$	14.6	11.4
$r \ge 130''$	7.5	5.1

TABLE 5

MEAN COLORS AND DISPERSIONS

Index	⟨Color⟩	N_{obj}	σ	$\langle\sigma_{obs}\rangle$	σ_0	⟨[Fe/H]⟩
			NGC 4472			
$B-V$	0.65	70	0.13	0.06	0.11	−1.61
$V-I$	1.09	70	0.18	0.10	0.15	−0.60
$B-I$	1.71	64	0.25	0.08	0.23	−1.15
			NGC 4649			
$B-V$	0.75	82	0.14	0.07	0.12	−1.11

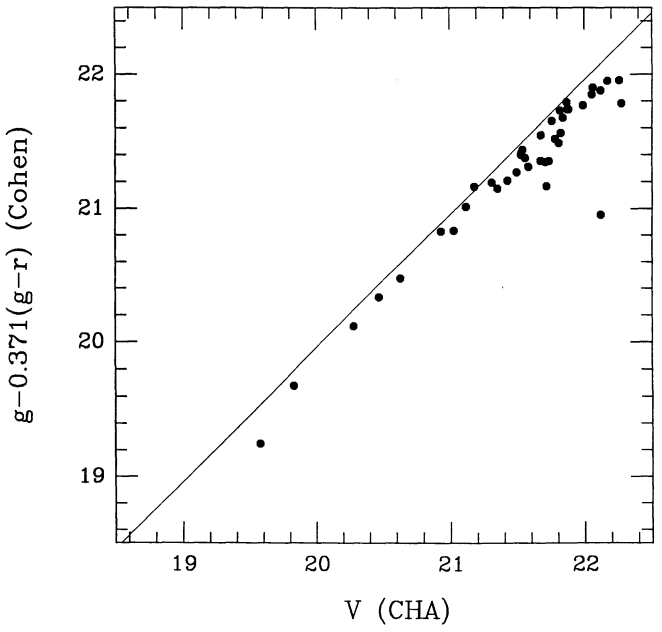

FIG. 2a

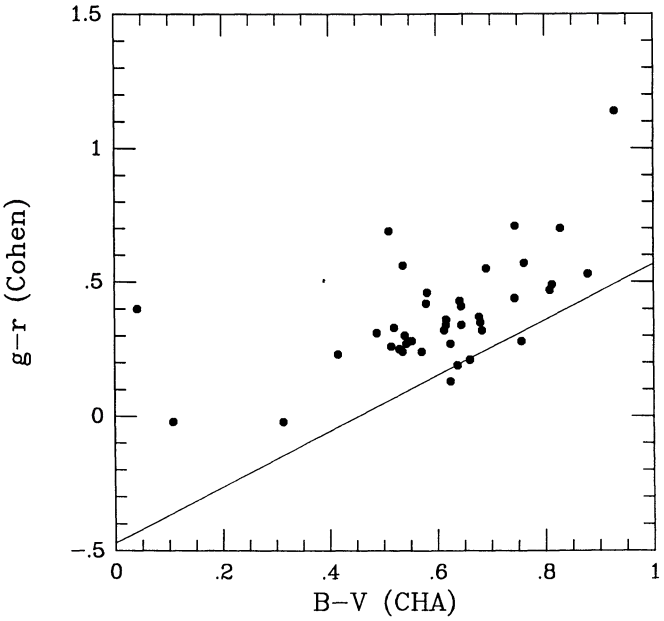

FIG. 2b

FIG. 2.—Comparison of our photometry with that of Cohen (1988) in the *gri* system. (*a*) Cohen's *g* magnitude, corrected for the standard color term described in the text, plotted against our measured *V* magnitude. (*b*) The $(g - r)$ color index plotted against our $(B-V)$. In both graphs, the solid line represents the standard transformation given by Cohen (1985).

ters in the calibrating samples of the Milky Way and M31 (e.g., Elson & Walterbos 1988, and Paper I). Note that we have shifted the $B-V$ range of NGC 4649 by 0.1 to take account of the mean color difference shown in Table 5.

The last column of Table 5 shows the metallicity deduced from the mean color of each system and the calibration of Paper I (the latter being the conversion of integrated color to metallicity, based on 65 Galactic globular clusters with low foreground reddenings). Foreground reddening to Virgo has been assumed to be zero (see Paper I).

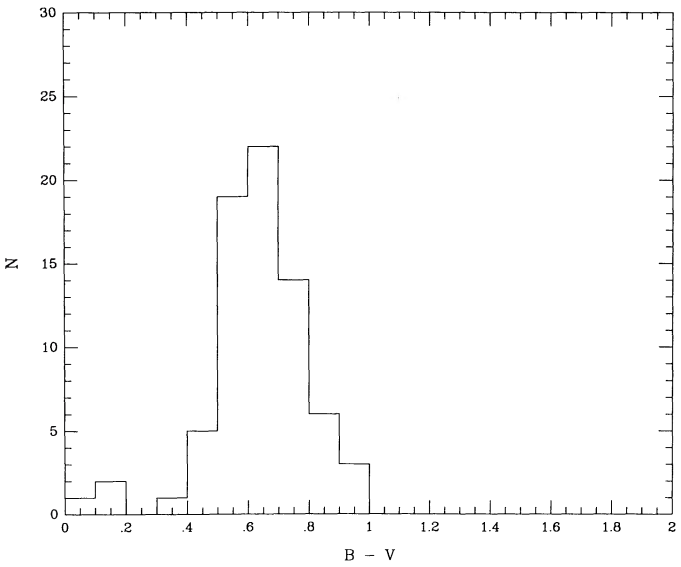

FIG. 3.—Histogram of $B-V$ values for the NGC 4472 clusters. *N* is the number of objects per 0.1 magnitude bin, and only objects brighter than $V = 22.5$ are plotted here and in the next three figures.

The [Fe/H] values for NGC 4472 from the three color indices are not consistent and require further comment. The larger-than-normal color scale uncertainty is an obvious possible cause for the discrepancy, since any calibration error would directly affect the mean colors and hence the metallicity deduced from them. For example, an arbitrary shift of $\simeq -0.1$ mag in our *V* zeropoint would almost completely reconcile all three metallicity values as well as producing closer agreement with the transformed Cohen scale described previously. Combined changes at the $\sim \pm 0.1$ mag level in all three bands could accomplish similar results. However, such zero-point shifts are 2–3 times larger than expected from the calibration uncer-

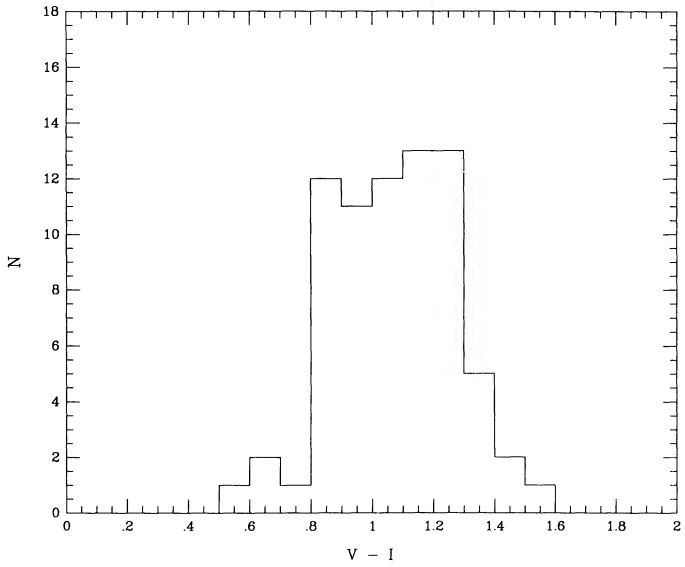

FIG. 4.—Histogram of $V-I$ values for the NGC 4472 clusters

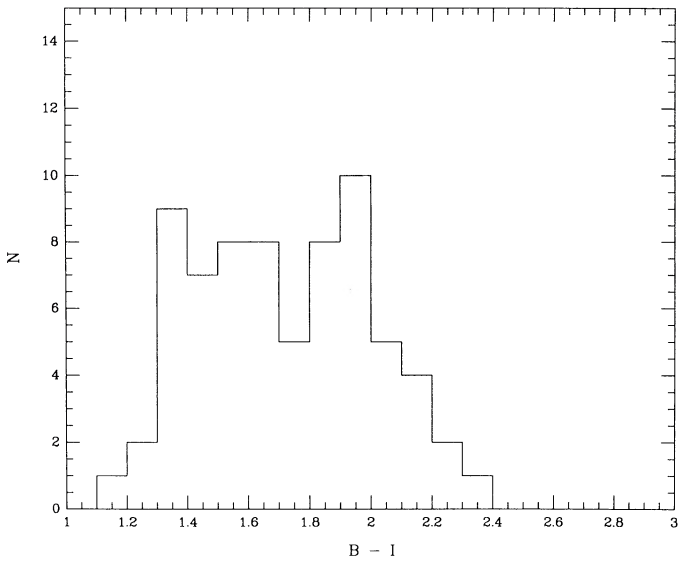

FIG. 5.—Histogram of $B - I$ values for the NGC 4472 clusters

tainties described in § 3 above; when these added in quadrature to the uncertainty of the mean $[\sigma/(N_{obj})^{1/2}]$, the net uncertainty would give σ[Fe/H] $\simeq \pm 0.3$ from either $B-V$ and $V-I$, or σ[Fe/H] $= \pm 0.2$ if we use $B-I$. Notice also the color-color distributions in Figures 7 and 8 for NGC 4472, along with the fiducial relations (see Paper I) for the Milky Way clusters. Clearly, the NGC 4472 distributions do not correspond to the Milky Way relations, by amounts that appear too large to be easily explained by intrinsic differences between the cluster populations (such as in mean age, or detailed abundance distributions; see, e.g., Burstein et al. 1984 or Paper I).

Although the resolution of this difficulty is not clear, as suggested previously we believe it is most likely due to a zeropoint error in at least one of our photometric bands. Thus for the present, in NGC 4472 we adopt the mean metallicity deduced from the $B-I$ index, which is less affected by scale uncertainties than the other two shorter-baseline colors (see, e.g.,

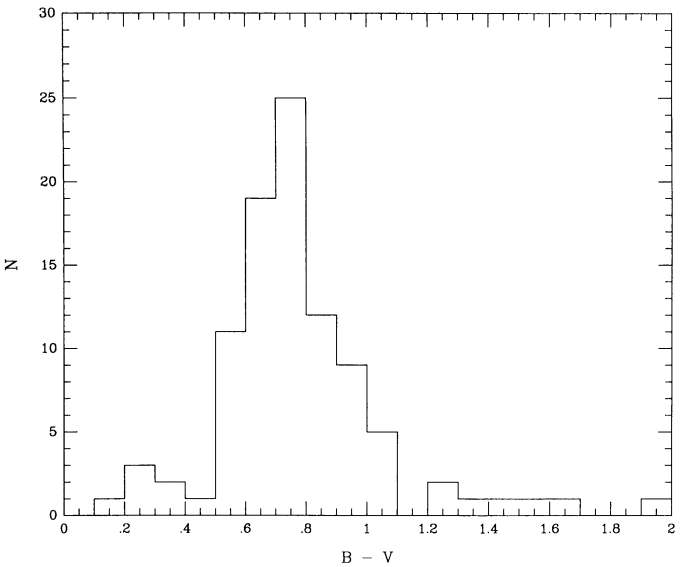

FIG. 6.—Histogram of $B - V$ values for the NGC 4649 clusters

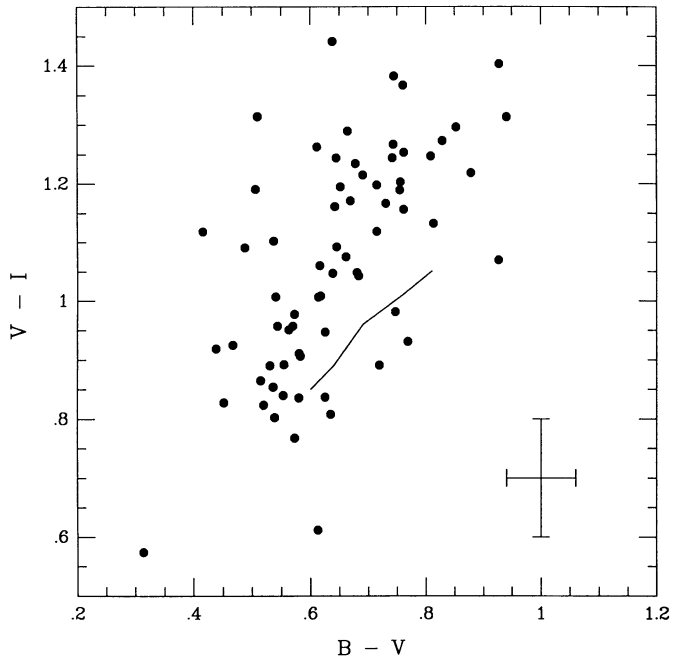

FIG. 7.—Color-color relation in $(V-I, B-V)$ for NGC 4472 clusters brighter than $V = 22.5$. The *solid line* is the intrinsic relation for the Milky Way globular clusters, from Reed et al. (1988). No reddening has been added to the Milky Way relation. The average uncertainty given by $\langle\sigma_{obs}\rangle$ in Table 5 is shown at lower right.

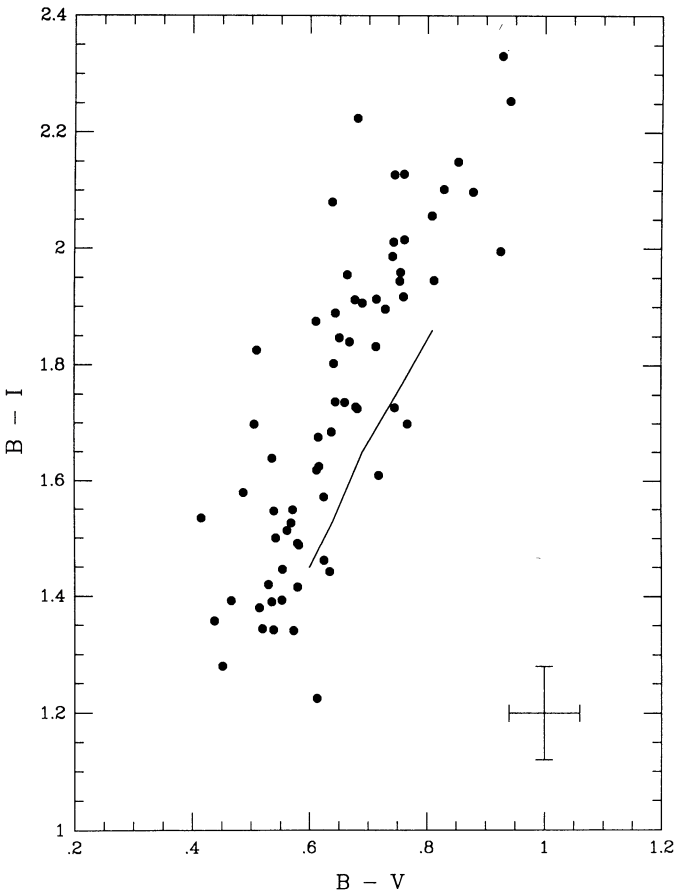

FIG. 8.—Color-color relation in $(B-I, B-V)$ for NGC 4472 clusters. Symbols are as defined in Fig. 7.

Geisler & Forte 1990 and Paper I). For NGC 4649, we are required to use $B-V$, the only index available. Thus for both galaxies, we estimate $\langle[Fe/H]\rangle \simeq -1.1$ for the overall metallicity of their globular clusters, essentially the same as for M87 and for Cohen's (1988) metallicity values from the *gri* indices in NGC 4472. For comparison, Mould et al. (1990) estimate $\langle[Fe/H]\rangle = -0.8 \pm 0.3$ for the NGC 4472 cluster system, from the median of the Mg *b* indices for 24 clusters. Recent photometric studies of the clusters in other giant elliptical galaxies such as NGC 5128 (Harris, Harris, & Hesser 1988) and NGC 1399 (Geisler & Forte 1990) have been published which indicate still redder colors corresponding to mean metallicity values $\langle[Fe/H]\rangle$ from -0.5 to -1. The variety of results, and their sensitivity to the photometric scale uncertainties, prevent any secure statements about general trends in the absolute metallicity distributions. However, the typical metallicities of the clusters in all these giant E galaxies are plainly higher by factors of ~ 2 or more than in the Milky Way halo (which has $\langle[Fe/H]\rangle_{MW} \sim -1.6$).

Unlike the mean metallicity, the metallicity *dispersion* from cluster to cluster depends only on color *differences* within the same field and thus is much more securely known. For NGC 4472, we obtain $\sigma[Fe/H] \simeq 0.6 \pm 0.1$ from each color. This value is very much the same for NGC 4649 and M87 (from Paper I) and is twice the range found for the globular clusters of the Milky Way halo ($\sigma[Fe/H] \sim 0.32$; see Zinn 1985). Our new data therefore support the conclusion discussed elsewhere (Cohen 1988; Geisler & Forte 1990; Paper I) that globular clusters in giant elliptical galaxies are more chemically enriched, and have a wider metallicity spread, than in the Milky Way.

5.2. *Distributions with Radius*

One of the main goals of this study is the investigation of radial trends in colors of globular cluster populations. Such gradients are present to differing degrees for the halo *light* in elliptical galaxies (e.g., Boroson & Thompson 1987; Franx, Illingworth, & Heckman 1989; and references therein) but they are often weak and difficult to measure well outside of the nucleus. Photometry of globular clusters offers an interesting alternative since their colors become *easier* to measure at larger radii, and they can be traced out to radial distances where the intensity of the halo light has fallen far below that of the sky background. Moreover, the radial *change* in the colors depends only on relative indices within the same field and is unaffected by the external zero-point uncertainties discussed in the previous section.

Any systematic radial trend, to be clearly detectable, must stand out over the large cluster-to-cluster dispersion in color. In several recent studies for a variety of large galaxies, the order of the day has generally been to find net gradients of color (metallicity) with radius that are weak or nonexistent. In the Milky Way halo, the dispersion itself, although distinctly smaller than in the elliptical galaxies discussed here, is certainly the dominant feature, and it has not been possible to establish whether or not the overall halo gradient is small-but-finite or actually zero (Zinn 1985; Harris 1990). For M31, the most recent and comprehensive analysis of the cluster colors (Elson & Walterbos 1988) suggests that once the inner metal-richest group of clusters is separated, the remaining halo group shows little or no net gradient in mean color with radius, and the clusters are systematically bluer [by $\Delta(B-V) \simeq 0.2$] than the spheroid. For a sample of bright clusters in the NGC 5128 halo, Hesser et al. (1984) find evidence for a small gradient in the usual sense that the reddest clusters are uniformly found closer to galaxy center, but Harris, Harris, & Hesser (1988) conclude from a larger sample that little or no color gradient can be seen. Finally, in M87 the photographically based study of Strom et al. (1981) reported a systematic decrease in the mean cluster color with increasing radius, but two subsequent CCD programs (Cohen 1988 and Paper I) have not confirmed this; instead, the color distributions appear almost perfectly constant with radius.

For NGC 4472 and 4649, we have divided our sample into four radial regions, each containing approximately the same number of objects. The mean and standard deviation for each region and color are listed in Table 6 (for NGC 4472) and Table 7 (for NGC 4649). The radial color distributions are also plotted in Figures 9–12, against log r. In each figure, the best linear regression is indicated by a straight line. As before, only objects with $V < 22.5$ are included in these plots, and, in addition, only those located in the color ranges defined in the previous section were used for computing the regression. Because the problem here is to determine the existence of an overall slope in the presence of considerable intrinsic scatter, we performed the regressions with a robust regression program (Press et al. 1986) which computes the median of the series of the two-point slopes of the sample instead of the mean. This algorithm assigns lower weight than normal least-squares routines to outlying points and thus is less sensitive to, e.g., sample contamination by foreground and background objects. The regressions we obtained for NGC 4472 (Figs. 9–11) are given

TABLE 6

COLOR DISTRIBUTION OF NGC 4472 GLOBULAR CLUSTERS

A. RADIAL DISTRIBUTION OF $B-V$

r limits	$\langle r\rangle$	$B-V$	σ_{sample}	N_{obj}	σ_{mean}
0″–60″	45″	0.70	0.14	18	0.03
60″–80″	72″	0.66	0.12	21	0.03
80″–95″	87″	0.63	0.12	17	0.03
>95″	113″	0.60	0.13	14	0.04

B. RADIAL DISTRIBUTION OF $V-I$

r limits	$\langle r\rangle$	$V-I$	σ_{sample}	N_{obj}	σ_{mean}
0″–60″	45″	1.15	0.21	18	0.05
60″–80″	73″	1.10	0.18	19	0.04
80″–95″	88″	1.03	0.14	18	0.03
>95″	113″	1.07	0.18	15	0.05

C. RADIAL DISTRIBUTION OF $B-I$

r limits	$\langle r\rangle$	$B-I$	σ_{sample}	N_{obj}	σ_{mean}
0″–60″	46″	1.79	0.27	16	0.07
60″–80″	72″	1.78	0.23	18	0.05
80″–95″	88″	1.62	0.18	16	0.05
>95″	114″	1.65	0.27	14	0.07

D. RADIAL DISTRIBUTION OF V

r limits	$\langle r\rangle$	V	σ_{sample}	N_{obj}	σ_{mean}
0″–60″	45″	21.77	0.47	18	0.11
60″–80″	72″	21.78	0.71	21	0.16
80″–95″	87″	21.91	0.47	17	0.11
>95″	112″	21.52	1.00	17	0.24

TABLE 7

COLOR DISTRIBUTION OF NGC 4649 GLOBULAR CLUSTERS

A. RADIAL DISTRIBUTION OF $B-V$

r limits	$\langle r \rangle$	$B-V$	σ_{sample}	N_{obj}	σ_{mean}
0″–55″	43″	0.85	0.15	23	0.03
55″–80″	66″	0.72	0.12	19	0.03
80″–105″	93″	0.72	0.13	18	0.03
>105″	123″	0.70	0.12	22	0.03

B. RADIAL DISTRIBUTION OF V

r limits	$\langle r \rangle$	V	σ_{sample}	N_{obj}	σ_{mean}
0″–55″	42″	21.82	0.52	29	0.10
55″–80″	66″	21.63	0.61	23	0.13
80″–105″	93″	21.93	0.39	20	0.09
>105″	123″	21.75	0.92	26	0.18

by the following expressions:

$$(B-V) = (-0.32 \pm 0.10) \log r + 1.25 ,$$

$$(V-I) = (-0.36 \pm 0.15) \log r + 1.75 ,$$

$$(B-I) = (-0.84 \pm 0.20) \log r + 3.27 ,$$

while the $(B-V)$ gradient we obtain for NGC 4649 (Fig. 12) is

$$(B-V) = (-0.32 \pm 0.11) \log r + 1.35 .$$

Just as for the other galaxies mentioned above, the color dispersion in each bin is larger than the change in mean color from bin to bin (see Tables 6 and 7). Nevertheless, gradients are evident to eye inspection of the diagrams, and are statistically significant at the $\sim 3\ \sigma$ level for each relation. For NGC 4472, the increased scatter in $(V-I)$ or $(B-I)$ apparent to the eye is likely to be an effect of the higher random errors in I (Table 1) compared with either B or V at the same brightness level.

Even though we believe that contribution of background objects is negligible (at the $\sim 10\%$ level or lower; see § 3), we simulated the effect that a population of blue background objects would have on the gradients. The presence of such a population could lead to an *artificial* color gradient even though the (redder) globular clusters might not have a radial color trend of their own. This gradient would be caused by the radial decrease in numbers of the cluster population (as $\sim r^{-1.5}$) occasioning a radial increase of the relative proportion of background objects. We simulated the color gradients resulting from different proportions of background objects, assuming the field population to have a mean color ~ 0.2 mag bluer in $B-V$ than the globular clusters. The results have been

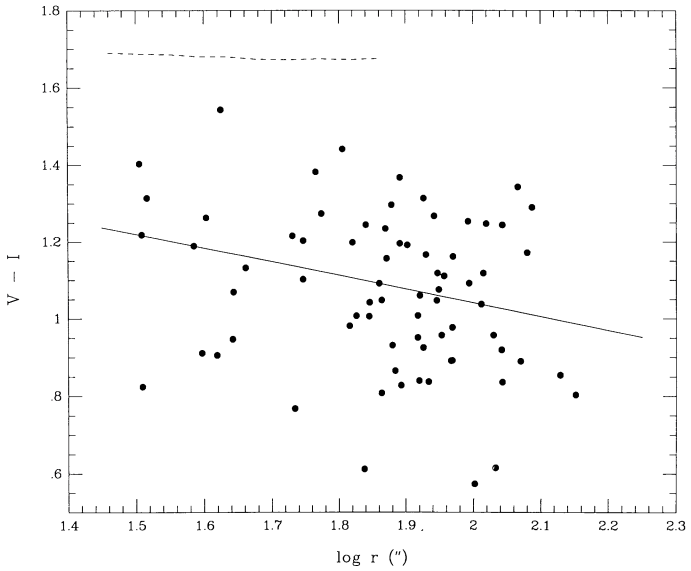

FIG. 10.—Radial $(V-I)$ color distribution for NGC 4472 globular clusters brighter than $V = 22.5$. The best linear regression excluding objects with $(V-I) < 0.7$ and $(V-I) > 1.6$ is indicated by the *solid line*. The integrated color profile of the NGC 4472 halo is indicated by the *dashed line*, from Bender & Möllenhoff (1987).

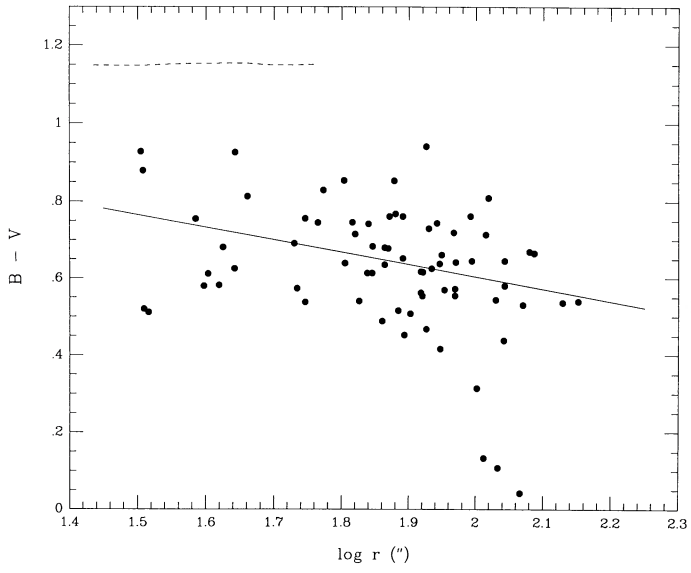

FIG. 9.—Radial $(B-V)$ color distribution for NGC 4472 globular clusters brighter than $V = 22.5$. The best linear regression excluding objects with $(B-V) < 0.4$ and $(B-V) > 1.0$ is indicated by the *solid line*. The integrated color profile of the NGC 4472 halo is indicated by the *dashed line*, transformed from the $(B-r)$ photometry of Boroson & Thompson (1987).

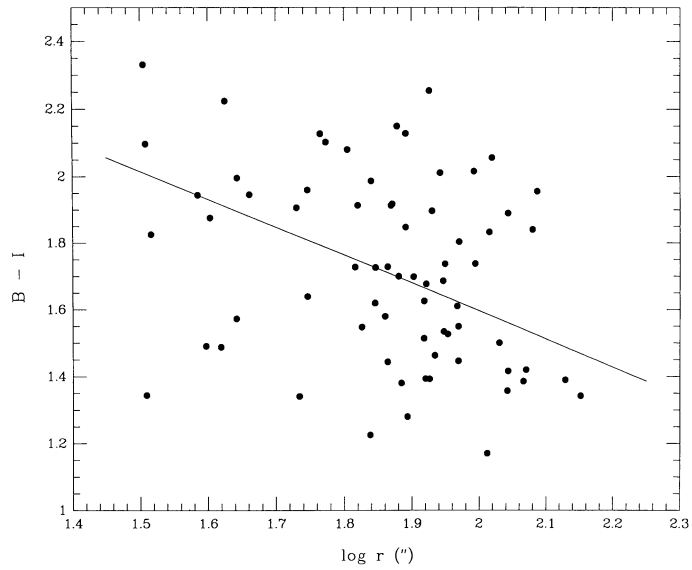

FIG. 11.—Radial $(B-I)$ color distribution for NGC 4472 globular clusters brighter than $V = 22.5$. The best linear regression excluding objects with $(B-I) < 1.3$ and $(B-I) > 2.2$ is indicated by the *solid line*.

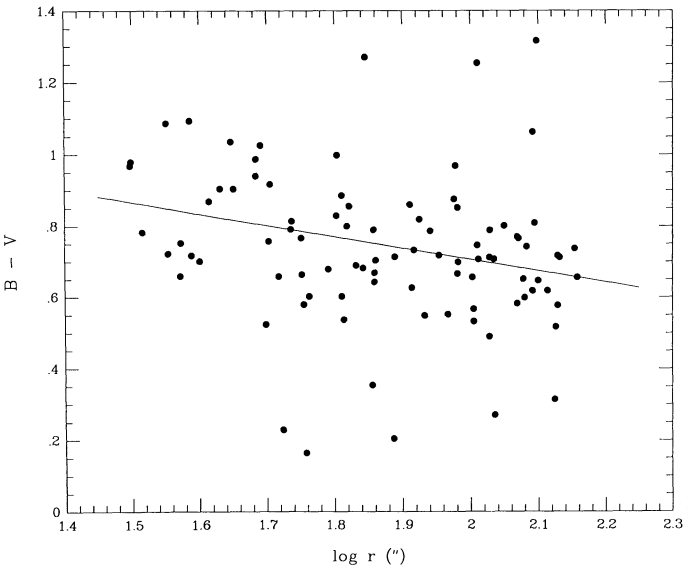

FIG. 12.—Radial $(B-V)$ color distribution for NGC 4649 globular clusters brighter than $V = 22.5$ The best linear regression excluding objects with $(B-V) < 0.3$ and $(B-I) > 1.2$ is indicated by the *solid line.*

discussed in Couture & Harris (1990). The main conclusion is that the maximum *false* gradient occurs when the contribution of background objects is ~40%. However, even at this contamination level, an intrinsic color gradient of $\Delta(B-V)/\Delta \log r = -0.2$ is required in the cluster population in order to reproduce the gradients that we actually see in NGC 4472 and NGC 4649. We conclude that realistic levels of background contamination are not sufficient to produce the observed color gradients.

The existence of significant color gradients is one of the primary results of this paper. By comparison, for NGC 4472 Cohen (1988) states that little or no radial changes in color index $(g-r,\ g-i)$ are seen over the range $30'' \lesssim r \lesssim 300''$, which is apparently at odds with our conclusion. Her statement is based on the median color and the first and third quartile points of the color histograms in each radial bin, rather than the mean regression of all the individual points as we use here; in the presence of significant background contamination the quartile points may be deceptively uniform. But more importantly, we note that plotting up Cohen's quoted *median* values against log r shows, in fact, a steady outward decline in color for both $(g-r)$ and $(g-i)$ that is statistically significant at the same level as we have found here. (Very much the same result appears to be true for the third galaxy she studies, NGC 4406, although the sample there is much smaller and the significance of the color gradient is lower. We also emphasize that in M87, Cohen's median color values indeed show no trend with radius for $r > 1'$, which we supported in Paper I. In short, the differences we find between M87 and NGC 4472 seem also to be detected in Cohen's data, which cover a larger radial range than ours.) Thus, we believe that Cohen's study and ours are actually in basic agreement: the central Virgo giant M87 system shows no internal color gradient, while the cluster systems in the more normal ellipticals NGC 4472, 4649, and (possibly) 4406 do possess gradients.

If composition differences are the primary factor causing these color gradients, then these two systems constitute the first clear detection of systematic radial metallicity variations in the globular cluster systems of normal large E galaxies. Furthermore, the total amplitude of the variations is surprisingly high. Using the calibration of Paper I to convert from color to [Fe/H], we find a total decrease in mean metallicity of Δ[Fe/H] $\gtrsim 0.5$ going outward from $r \sim 4$ to 10 kpc (~ 1.6–2.0 in log r). It is interesting to note that the amplitude of these gradients is very much the same as in the Milky Way over the same radial region (4–10 kpc), if we *include* the "metal-rich" globular clusters now usually regarded to be a disklike system (Zinn 1985; Armandroff 1989). In our opinion, it is not obvious whether or not we should compare the clusters we find in elliptical galaxies with *only* the halo clusters in our Galaxy, or with *all* the known Galactic globular clusters, since the clusters in the giant ellipticals evidently extend up to near-solar metallicity.

The color gradient of the *halo* light of NGC 4472 is shown in Figures 9–10 (*dashed lines*). Here, the $B-V$ data come from the $B-r$ surface photometry of Boroson & Thompson (1987) to which we applied Cohen's transformations (see § 4 above), while $V-I$ is drawn from Bender & Möllenhoff (1987). Just as for M87, the most straightforward feature is the clear difference in color between the mean halo color and the globular clusters. Even taking in account the zero-point uncertainty in our color scales, the clusters are systematically bluer than the halo by $\Delta(B-V) \gtrsim 0.2$, corresponding to Δ[Fe/H] $\gtrsim 0.4$ if due to metallicity alone. A second notable feature is the absence of clear color gradients in the halo over the radial range of overlap with the clusters. In fact, weak color gradients do exist in many galaxy spheroids, mostly apparent near the center of the galaxies (inside the main region plotted here in Figs. 9 and 10). For the study of metallicity gradients in halos and spheroids, which represent a considerably larger and more uncertain mix of stars than do the clusters, observations of line strength gradients are more relevant than broad-band colors. Spectroscopically based metallicity gradients at the level of Δ[Fe/H]$/\Delta \log (r/r_e) \sim -0.25$ (where r_e is the effective radius) have been detected for several halos and bulges of elliptical galaxies (Couture & Hardy 1988; Gorgas, Efstathiou, & Salamanca 1990; and references therein). Even though a large scatter around this value, these gradients are clearly less steep (by a factor of at least 4) than those we are reporting for the globular cluster systems here.

We have looked for any radial or color variations in our data against V magnitude (i.e., cluster luminosity). The summary of mean points in Tables 6 and 7 indicates no such trend. In addition, the mean magnitude and the dispersion of the inner region are entirely similar to those of the other regions, suggesting that the photometry has not been systematically affected by the brighter halo light of the galaxies there. In Figures 13 and 14 we show the distribution of globular clusters in $(V, B-V)$. Except for the expected increase of color dispersion at the faintest magnitudes with the increased photometric uncertainty, no systematic trend of color with luminosity is seen. The same conclusion has been reached for other galaxies (Cohen 1988; Geisler & Forte 1990; Harris et al. 1988; Paper I).

The observation that the clusters are distinctly bluer than the halo is one of the major pieces of evidence that the globular cluster systems in these galaxies may be somewhat older than the rest of the halo, belonging to a more spatially extended and less enriched epoch (Strom et al. 1981; Harris 1986). Our new data add further to the photometric evidence which points in this direction. Perhaps the more surprising result of our study is the detection of color gradients in the two cluster systems. A

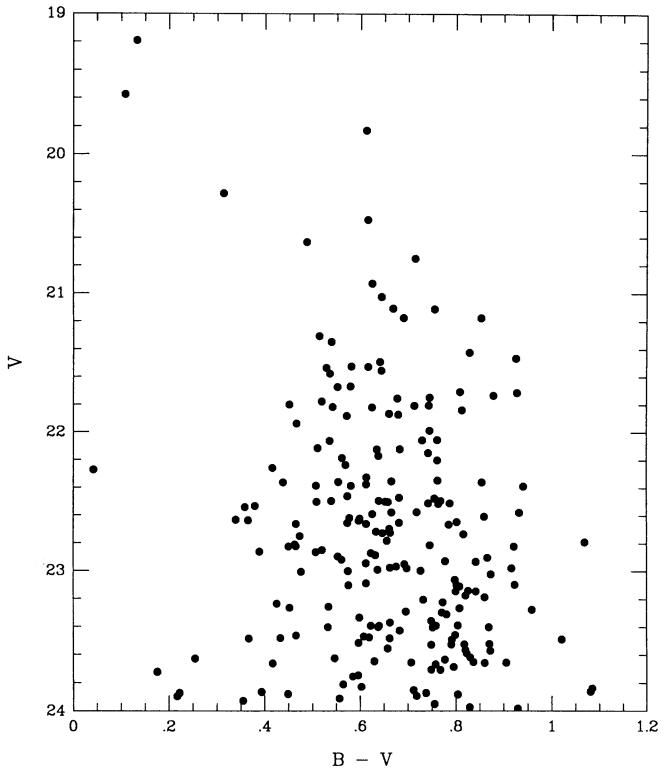

FIG. 13.—Apparent V magnitude against $B-V$ for NGC 4472 globular clusters. All our measured sample contained in Table 2 is shown.

strong metallicity gradient is classically more consistent with the picture of galaxy formation via dissipative collapse in a more-or-less single process, or else by the merger of gas-rich fragments which could then collapse further and self-enrich more in the center than the low-density outskirts of the system (e.g., Eggen, Lynden-Bell, & Sandage 1962; Sandage & Fouts 1987; Larson 1975; Gott 1977; Gilmore, Wyse, & Kuijken 1989; Lake & Carlberg 1988; Kormendy 1989; Carney, Latham, & Laird 1990).

The alternate view of forming large E galaxies by mergers of existing galaxies is, however, not ruled out. Recent simulations (Barnes 1988, 1989) show that overall halo gradients can be preserved when two disk galaxies merge. Thus, since the color gradients in globular cluster systems of the Milky Way and M31 are similar to those found in NGC 4472 and 4649, the merger of such two spiral galaxies remains a possibility. For galaxies with no metallicity gradients, a wider range of formation processes would be feasible, involving the amalgamation of many small subsystems rather than two or three larger ones (e.g., Searle & Zinn 1978; Kormendy 1989; Lee, Demarque, & Zinn 1990; and the references cited above). M87, in which no color gradient whatsoever was found, then seems to be a more likely candidate for having been built or largely altered by merger processes.

Recently, Bridges, Hanes, & Harris (1990) have found that the central Fornax giant NGC 1399 also possesses a radial color gradient in its globular cluster system, of virtually the same amount [$\Delta(B-V) \simeq 0.1$] over the same galactocentric distance range that we studied here. What is additionally fascinating (and perplexing) is that NGC 1399 is a cD-type central giant elliptical, with the same high specific-frequency anomaly that M87 has. Thus, it might be expected to be an even more likely candidate for buildup by merger processes, so that the existence of a strong metallicity gradient in the cluster system (but perhaps not the halo light! see the discussion cited) is especially surprising. As yet, we have no satisfactory interpretation which ties together all of these observations.

As has been argued from other directions (see, e.g., Kormendy 1989), the evidence from globular cluster systems therefore seems to suggest that giant E galaxies formed in more than one way. It is all the more remarkable that the globular clusters in these galaxies resemble each other so closely in luminosity (Harris et al. 1991) and in spatial distribution (Harris 1986); the radial color gradients now seem to be one of the very few ways that distinct differences in their cluster systems can arise (the specific frequencies are another).

Although the multicolor photometry is most easily interpreted in terms of metallicity differences between clusters—and between the mean of the clusters and the halo—the ages of the clusters must also be a factor. The cluster colors vary with age in a way that itself depends on metallicity (e.g., Searle, Sargent, & Bagnuolo 1973; Searle, Wilkinson, & Bagnuolo 1980; van den Bergh 1981; Elson & Walterbos 1988; Chiosi, Bertelli, & Bressan 1988), and with only one or two broad-band indices age and abundance changes cannot be definitively separated. Increased age could, for example, be responsible for some part of the bluer cluster colors relative to the surrounding halo light, because of the shift of the horizontal-branch stars in the clusters toward higher temperature with advancing age (see Rood 1973; Sweigart, Renzini, & Tornambè 1987). However, what makes this alternative so unattractive is simply that *very* large age differences (5 Gyr and more) are needed to produce systematic color changes of $\Delta(B-V) \simeq 0.1$–0.2 mag for clusters

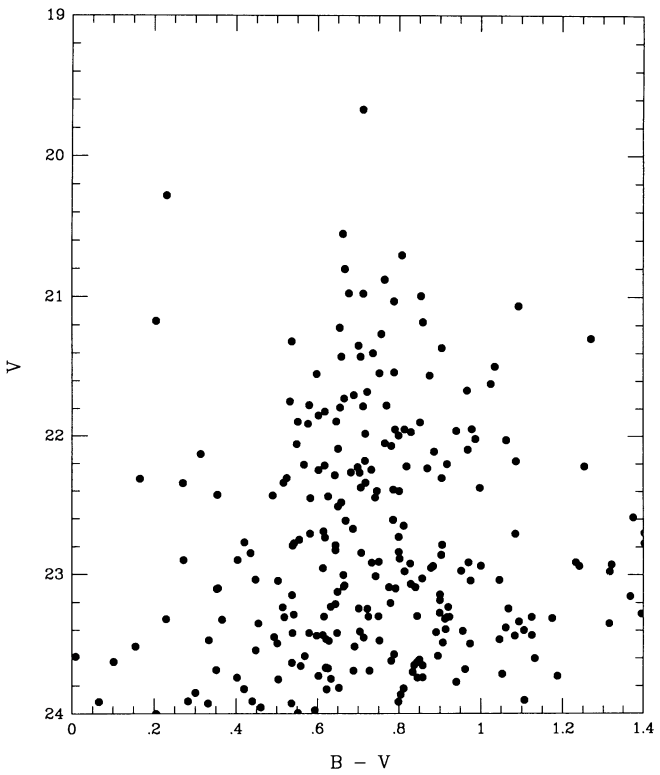

FIG. 14.—Apparent V magnitude against $B-V$ for NGC 4649 globular clusters. All our measured sample contained in Table 3 is shown.

that are already old. By contrast, quite plausible metallicity differences between clusters will produce the same color changes at constant age, and the mean cluster metallicities derived by the broad-band indices are supported by existing spectroscopic material (e.g., Hanes & Brodie 1986; Mould, Oke, & Nemec 1987; Mould et al. 1990). Population synthesis from high signal-to-noise spectra of a selected sample of clusters in these galaxies could largely help to disentangle these two effects.

6. SUMMARY

1. The mean colors of the globular clusters in NGC 4472 and NGC 4649 suggest a mean metallicity of [Fe/H] ~ -1.1 for their cluster systems, noticeably higher than for the clusters of the Milky Way halo ([Fe/H] ~ -1.6). This difference suggests that the star formation rate and/or the recycling of processed matter were more efficient in elliptical galaxies at the time of cluster formation. The cluster systems in all three of NGC 4472, NGC 4649, and M87 (Paper I) have similar metallicity, although this last result is subject to confirmation of our photometric scales.

2. The mean colors of the NGC 4472 globular clusters are clearly bluer than its halo, by several tenths of a magnitude in both $(B-V)$ and $(V-I)$. This result strongly supports what has been found for other large galaxies, both spiral and elliptical, and argues in favor of a distinct and early epoch of formation for globular clusters. It seems also unlikely that the halos of these galaxies were substantially formed from the disruption of such globular clusters.

3. At any radius, the range in colors of the clusters is large (corresponding to Δ[Fe/H] > 1.5) and covers nearly all the metallicity range present in globular clusters of our Galaxy. The dispersion around the mean metallicity (σ[Fe/H] ~ 0.6) is also twice as large as in the globular cluster system in the halo of the Milky Way. As in Paper I, these results suggest that the range in physical conditions at the time of cluster formation was significantly larger in the giant E galaxies than in the Milky Way.

4. For the first time, a clear radial trend in mean color has been found for globular cluster systems in at least *some* normal elliptical galaxies, presumably representative of a metallicity gradient. In this respect, NGC 4472 and 4649 differ clearly from M87, in which little or no gradient exists. An interpretative picture is therefore favored in which the relative importance of mergers versus dissipitative collapse can vary among galaxies that today look structurally similar.

We gratefully acknowledge financial support through the Natural Sciences and Engineering Research Council of Canada, the National Research Council, and the Fonds FCAR du Québec.

REFERENCES

Ables, H. A., Newell, E. B., & O'Neil, E. J. 1974, PASP, 86, 311
Armandroff, T. E. 1989, AJ, 97, 375
Barnes, Joshua E. 1988, ApJ, 331, 699
———. 1989, in Dynamics and Interactions of Galaxies, ed. R. Wielen (Heidelberg: Springer-Verlag), in press
Bender, R., & Möllenhoff, C. 1987, A&A, 177, 71
Boroson, T. A., & Thompson, I. B. 1987, AJ, 93, 33
Bridges, T., Hanes, D. A., & Harris, W. E. 1990, AJ, in press
Burstein, D., Faber, S. M., Gaskell, C. M., & Krumm, N. 1984, ApJ, 287, 586
Carney, B. W., Latham, D. W., & Laird, J. B. 1990, AJ, 99, 572
Chiosi, C., Bertelli, G., & Bressan, A. 1988, A&A, 196, 84
Cohen, J. G. 1985, AJ, 90, 2254
———. 1988, AJ, 95, 682
Couture, J., & Hardy, E. 1988, AJ, 96, 867
Couture, J., & Harris, W. E. 1990, Proc. ASP Conf. in Formation and Evolution of Star Clusters, ASP, in press.
Couture, J., Harris, W. E., & Allwright, J. W. B. 1990, ApJS, 73, 671
Eggen, O. J., Lynden-Bell, D., & Sandage, A. 1962, ApJ, 136, 748
Elson, R. A. W., & Walterbos, R. A. M. 1988, ApJ, 333, 594
Forte, J. C., Strom, S. E., & Strom, K. M. 1981, ApJ, 245, L9
Franx, M., Illingworth, G., & Heckman, T. 1989, AJ, 98, 538
Geisler, D., & Forte, J. C. 1990, ApJ, 350, L5
Gilmore, G., Wyse, R. F. G., & Kuijken, K. 1989, ARAA, 27, 555
Gorgas, J., Efstathiou, G., & Salamanca, A. 1990, preprint
Gott, J. R. 1977, ARAA, 15, 235
Grillmair, C. J., Pritchet, C. J., & van den Bergh, S. 1986, AJ, 91, 1328
Hanes, D. A. 1971, M.Sc. thesis, University of Toronto
———. 1977, Mem. R.A.S., 84, 45
Hanes, D. A., & Brodie, J. P. 1986, ApJ, 300, 279
Harris, H., Harris, G. L. H., & Hesser, J. E. 1988, in IAU Symposium 126, Globular Cluster Systems in Galaxies, ed. J. E. Grindlay & A. G. D. Philip (Dordrecht: Kluwer Academic), 205
Harris, W. E. 1986, AJ, 91, 822
Harris, W. E. 1988, in IAU Symposium 126, Globular Cluster Systems in Galaxies, ed. J. E. Grindlay & A. G. D. Philip (Dordrecht: Kluwer Academic), 237
———. 1990, in ESO/CTIO Conf. on Galactic Bulges, ed. B. Jarvis & D. Terndrup (Garching: ESO Conf. Ser), 153
Harris, W. E., Allwright, J. W. B., Pritchet, C. J., & van den Bergh, S. 1991, ApJS, in press
Harris, W. E., & van den Bergh, S. 1981, AJ, 86, 1627
Hesser, J. E., Harris, H. C., van den Bergh, S., & Harris, G. L. H. 1984, ApJ, 276, 491
Kormendy, J. 1989, ApJ, 342, L63
Lake, G., & Carlberg, R. 1988, AJ, 96, 1581
Landolt, A. U. 1973, AJ, 78, 959
———. 1983, AJ, 88, 439
Larson, R. B. 1975, MNRAS, 173, 671
Lee, Y.-W., Demarque, P., & Zinn, R. 1990, ApJ, 350, 155
Mould, J. R., Oke, J. B., de Zeeuw, P. T., & Nemec, J. M. 1990, preprint
Mould, J. R., Oke, J. B., & Nemec, J. M. 1987, AJ, 93, 53
Press, W. H., Flannery, B. P., Teukolsky, S. A., & Vetterling, W. T. 1986, Numerical Recipes (Cambridge: Cambridge University Press)
Pritchet, C. J., & van den Bergh, S. 1987, ApJ, 318, 507
Reed, B. C., Hesser, J. E., and Shawl, S. J. 1988, PASP, 100, 545
Rood, R. 1973, ApJ, 184, 815
Sandage, A., & Fouts, G. 1987, AJ, 93, 592
Schild, R. 1983, PASP, 95, 1021
Searle, L., Sargent, W. L. W., & Bagnuolo, W. G. 1973, ApJ, 179, 427
Searle, L., Wilkinson, A., & Bagnuolo, W. G. 1980, ApJ, 239, 803
Searle, L., & Zinn, R. 1978, ApJ, 225, 357
Stetson, P. B. 1987, PASP, 99, 191
Strom, S. E., Forte, J. C., Harris, W. E., Strom, K. M., Wells, D. C., & Smith, M. G. 1981, ApJ, 245, 416
Sweigart, A. V., Renzini, A., & Tornambè, A. 1987, ApJ, 312, 762
van den Bergh, S. 1981, A&AS, 46, 79
Zinn, R. 1985, ApJ, 293, 424